Earth Planets Space, **65**, 725–730, 2013

S_n velocity tomography beneath the Himalayan collision zone and surrounding regions

Yan Lü[1,2], Bin Liu[2], Sidao Ni[3,2], and Shunping Pei[4]

[1]*Institute of Geology and Geophysics, Chinese Academy of Sciences, Beijing 100029, China*
[2]*School of Earth and Space Sciences, University of Science and Technology of China, Hefei 230026, China*
[3]*Key Laboratory of Dynamical Geodesy, Institute of Geodesy and Geophysics, Chinese Academy of Sciences, Wuhan 430077, China*
[4]*Key Laboratory of Continental Collision and Plateau uplift, Institute of Tibetan Plateau Research, Chinese Academy of Sciences, Beijing 100085, China*

(Received June 11, 2012; Revised December 23, 2012; Accepted December 25, 2012; Online published August 23, 2013)

We present a tomographic S_n velocity model of the uppermost mantle beneath the Himalayan collision zone and surrounding regions. A total of 43,905 S_n phases are used in the investigation. The average S_n velocity in the study area is approximately 4.6 km/s, and the velocity perturbations reach 0.2 km/s. The S_n velocity distribution is consistent with P_n tomography results obtained previously. High velocities are found under the Indian plate, the Tarim Basin, and the Sichuan Basin, whereas low S_n velocities are found beneath the Myanmar region, the Hindu–Kush region, and the Lhasa block and western Qiangtang block. These results support the idea that the lithosphere of the Indian plate is subducted into the mantle and causes the upwelling of hot material. The east–west variability of the S_n velocity beneath the Indian plate and southern Tibet indicates that the underthrusting of the Indian continental lithosphere may be in a piecewise manner. The differences between the thermal structure of the crust and upper mantle in southern Tibet suggest that this region may be represented by a tectonic model of hot crust and cold mantle, supporting the idea that crustal material flow may occur in this region.
Key words: S_n, velocity, tomography, Indian plate.

1. Introduction

The collision between the Indian and Eurasian plates is one of the most important global continent–continent plate collisions. This phenomenon has an extremely important impact on the tectonics of the Himalayan collision zone and the surrounding regions (Fig. 1). The tectonics of this area is active and has a complex structure, and is one of the hotspots of Earth science research (Molnar and Tapponnier, 1975; Teng *et al*., 1994, 1999; Zeng *et al*., 2000; Wang *et al*., 2001; Zhang and Klemperer, 2010; Zhang *et al*., 2010a, b, 2011). This subject was the focus of a number of previous studies (Kind *et al*., 2002; Ding *et al*., 2003; Hearn *et al*., 2004; Liang *et al*., 2004; Zhao, 2004; Liang and Song, 2006; Pei *et al*., 2007, 2011a, b; Phillips *et al*., 2007; Xu *et al*., 2007; Ren and Shen, 2008; Sun *et al*., 2008; Lü *et al*., 2011; Yue *et al*., 2012). The P_n velocity inversion indicates that the Indian plate has a relatively high P_n velocity, whereas areas in Afghanistan, Myanmar, and the Tibetan Plateau are low P_n velocity zones. The subduction of the Indian plate lithosphere to the mantle of the Hindu–Kush and Myanmar regions is widely accepted (Zang *et al*., 1992), but the specific characteristics of the collision and movement under the Tibetan Plateau are still unclear. Ding *et al*. (2003) provided Cenozoic volcanism evidence for the transition from oceanic to continental subduction in Tibet. The INDEPTH-III study proposed that the lower lithosphere of the Indian plate subducts northward at a larger angle (Zhao *et al*., 2004). The model proposed by Liang and Song (2006) considers that the crust of the Indian plate subducts under the crust of the Eurasian plate and above the mantle. Huang and Zhao (2006), as well as Zheng *et al*. (2007), proposed that the Indian plate lithosphere subducts 200–300 km deep into the mantle by teleseismic P-wave inversion. Using the receiver function method, Yue *et al*. (2012) interpreted either a piece of the Lhasa Terrane or a remnant oceanic slab underthrust below northern Tibet. However, the mechanism of subduction is still unclear and requires further examination.

The S_n velocity at the uppermost mantle is significantly influenced by the temperature, pressure, and material composition. The effect of temperature change is more pronounced on the S wave velocity than on the P wave velocity. In high-temperature regions where partial melting is present, the S wave velocity decreases more significantly than the P wave velocity (Nolet and Ziehuis, 1994; Goes *et al*., 2000). Therefore, the S_n velocity distribution can provide more evidence of the thermal situation and plate movement characteristics of the study region. Previous studies using waveform records found S_n wave propagation attenuation under the Tibetan plateau (Ni and Barazangi, 1983; Rapine *et al*., 1997). However, these previous S_n wave studies were influenced by the amount of data, and there are fewer high-resolution inversion results. In the current work, we present an S_n velocity tomographic model using a large number of S_n travel-time data obtained from the Inter-

doi:10.5047/eps.2012.12.012

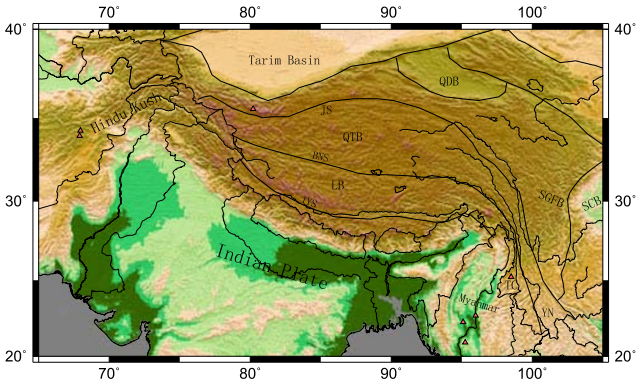

Fig. 1. Simplified tectonic map of the Himalayan collision zone and adjacent regions superimposed on topography from Lü *et al.* (2011). BNS, Bangong–Nujiang suture; IYS, Indus–Yarlung Zangbo suture; JS, Jinsha River suture; LB, Lhasa Block; QDB, Qaidam Basin; QTB, Qiangtang Block; SCB, Sichuan Basin; SGFB, Songpan–Ganzi fold belt; TC, Tengchong volcano; YN, Yunnan. Triangles denote volcanoes; black lines represent the tectonic line.

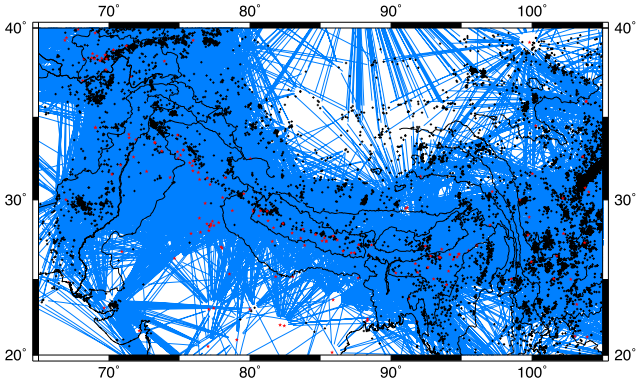

Fig. 2. Ray paths for S_n travel times. From 9716 events recorded by 327 stations, 43,905 S_n rays were obtained. Events are represented by black crosses and stations are indicated by red stars.

national Seismological Centre, the China Earthquake Data Center, and the Annual Bulletin of Chinese Earthquakes. This S_n velocity model provides more insight into the plate tectonic features of the study region.

2. Data and Method

Our study area is located at 20°–40°N and 65°–105°E. Seismic data from 9716 events recorded by 327 stations located at 10°–50°N and 55°–115°E are used. These S_n travel-time data are from three sources, namely, the International Seismological Centre (1960–2007), the China Earthquake Data Center (1990–2009), and the Annual Bulletin of Chinese Earthquakes (1985–2011). The arrival times from the China Earthquake Data Center and the Annual Bulletin of Chinese Earthquakes are picked by the technicians of China Earthquake Administration using a conventional method, based on information of the seismic amplitude with aid from the forward arrival time. For the inversion, we used S_n data for which the epicenter distance ranged between 2° and 10°. The initial models were obtained by a linear fit to the travel-time-distance curve. The average S_n velocity is 4.6 km/s. The crustal thickness of the initial model is 50 km and the mean shear wave velocity of the crust is 3.6

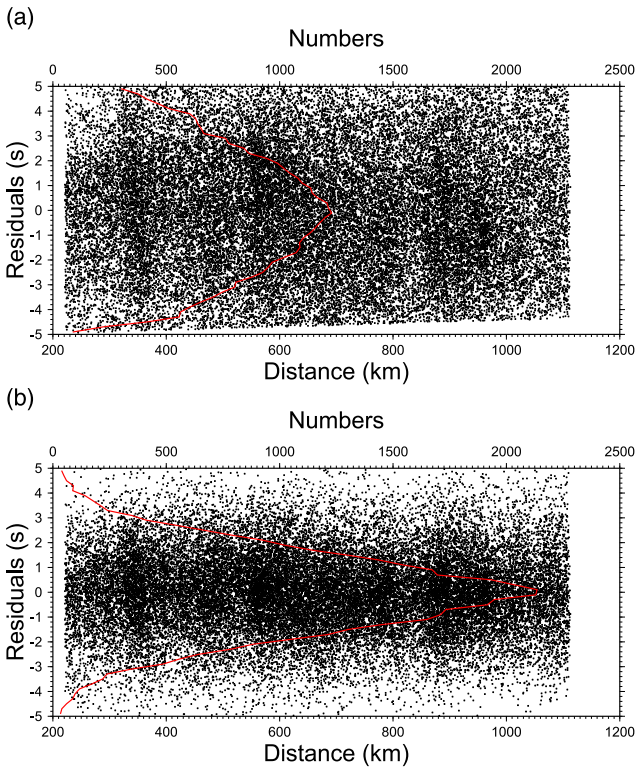

Fig. 3. Distribution of residuals versus epicentral distance before (Fig. 3(a)) and after (Fig. 3(b)) inversion. The standard deviation of S_n travel time residuals is 2.8 s for the original data, decreasing to 1.5 s after inversion. The red lines are histograms with 0.2 s residuals of the bin width.

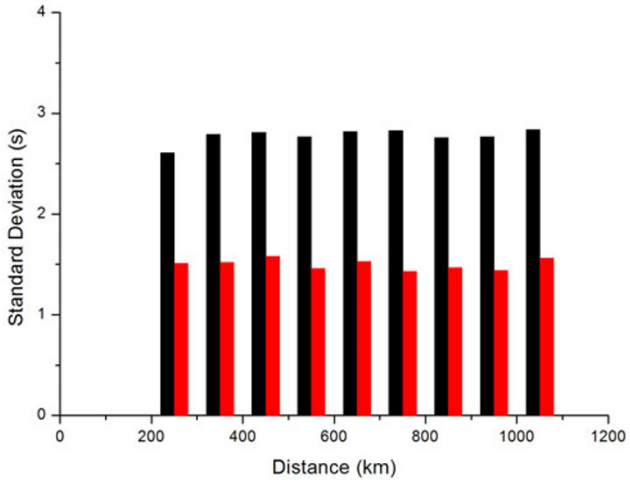

Fig. 4. Histograms of the standard deviations as a function of distance. Black and red columns indicate the standard deviation of S_n travel-time residuals before, and after, the inversion, respectively.

km/s. The travel time residuals (difference between predicted and reported travel times) used are limited to a range of ±5 s, giving a total of 43,905 S_n rays. The source/station ray paths are shown in Fig. 2.

We followed the tomography technique proposed by Hearn (1996). The uppermost layer of the mantle is divided into a set of two-dimensional cells in which the slownesses (inverse velocities) are estimated. The S_n travel time residuals are approximately described by the perturbation equa-

tion:

$$t_{ij} = a_i + b_j + \sum d_{ijk} S_k, \quad (1)$$

where t_{ij} is the travel-time residual for event j and station i, a_i is the static delay for station i, b_j is the static delay for event j, d_{ijk} is the travel distance of ray ij in mantle cell k, and S_k is the slowness perturbation for cell k. The average velocity $\bar{V}$ is obtained by fitting the travel time and epicentral distance. The velocity perturbation is given by $-\bar{V} \times \bar{V} \times S_k$. The unknown quantities in Eq. (1) are the mantle slowness perturbation S_k, the station delay a_i, and the event delay b_j. The station and event delays accommodate variations in crustal velocity and thickness, as well as source uncertainties. In solving the set of travel-time equations, we use a cell size of $30' \times 30'$. The slowness values in each cell are resolved by the LSQR algorithm (Paige and Saunders, 1982; Yao *et al.*, 1999). A damping constant of 600 is used to control the smoothness of the velocity image by damping the slowness variations. The rms residuals of the S_n travel times decrease from 2.8 s to 1.5 s after inversion (Figs. 3 and 4). Compared with P_n anisotropy, the anisotropy of the S_n wave is more complicated due to the presence of shear-wave splitting, which cannot be expressed by the P_n velocity and anisotropy inversion method. Only the S_n velocity tomographic model is used in the present study. According to research into the P_n velocity and anisotropy joint inversion (Lü *et al.*, 2012), although the two velocity models are slightly different in details depending on whether, or not, anisotropy is considered, the major velocity pattern variations are similar.

3. Checkerboard Test

Checkerboard tests were conducted to evaluate the effects of ray coverage on the spatial resolution. A test checkerboard velocity model was created by assigning sinusoidal S_n velocity anomalies to the cells of the model. The average amplitude (max $\Delta v/\sqrt{2}$) of the sinusoidal velocity is 0.2 km/s. Synthetic arrival times were calculated for the test model under different checkerboard sizes of velocity with the same number of earthquakes, stations, and ray paths as those used in the tomographic inversion of the real data. Gaussian noise with a standard deviation of 1.5 s (equal to the rms residuals after inversion) was added to the synthetic travel times and noise with a standard deviation of 15 km was added to the event locations to perform the pick errors, source uncertainties, and other noises (Pei and Chen, 2012). Figure 5 shows the checkerboard test results. The tests indicate that, for most of the study area, $3^\circ \times 3^\circ$ cells for S_n velocity can be resolved well. The ray coverage is high at the Himalayan collision zone, the eastern and western Himalayan syntaxis, and surrounding regions, and the spatial resolution there can reach $2.5^\circ \times 2.5^\circ$, or even better. Our spatial resolution is considered to be good for the focus areas and better than a previous study (Pei *et al.*, 2007).

4. Results and Discussion

Figure 6 shows the station delays after inversion using real data. The station delay terms are related to crustal thickness, crustal velocity, and surface geology. However, the crustal thickness is the dominant factor that affects the station delays. We can see that in areas with thick crusts,

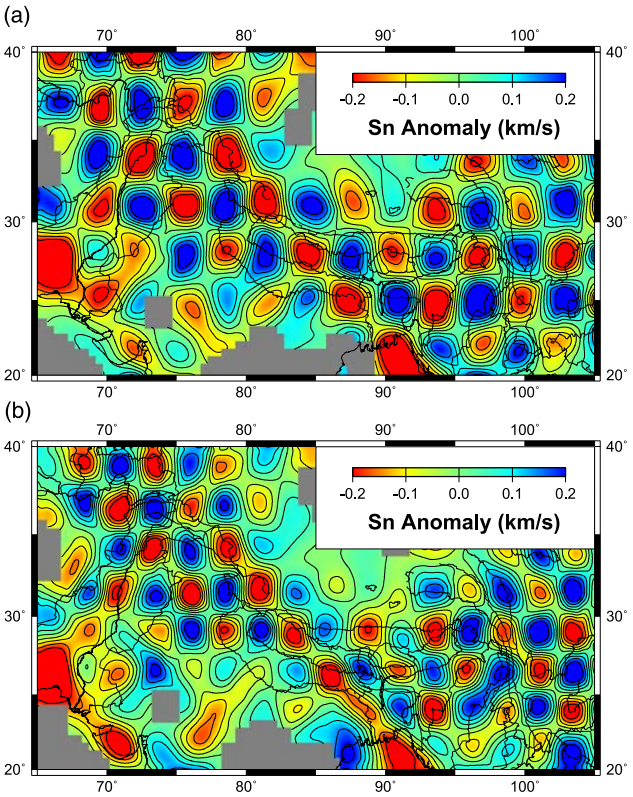

Fig. 5. Checkerboard test result for the $3^\circ \times 3^\circ$ sinusoidal velocity model (Fig. 5(a)) and test result for the $2.5^\circ \times 2.5^\circ$ model (Fig. 5(b)). The isopleths point to ± 0.2, ± 0.15, ± 0.1, ± 0.05, and 0.0 km/s velocity anomalies.

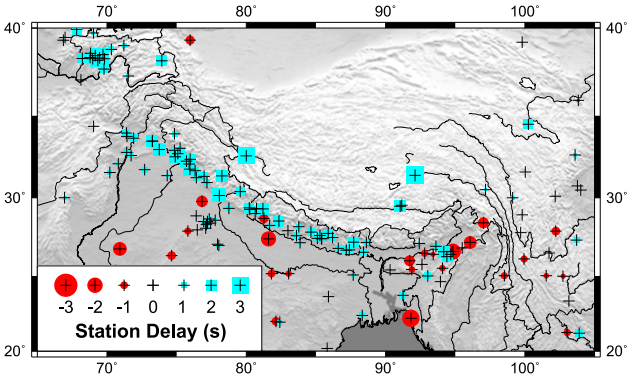

Fig. 6. Station delay (in seconds) for S_n travel times. Crosses represent stations. Circles indicate early arrival times, and squares indicate late arrival times. The sizes are proportional to the delay.

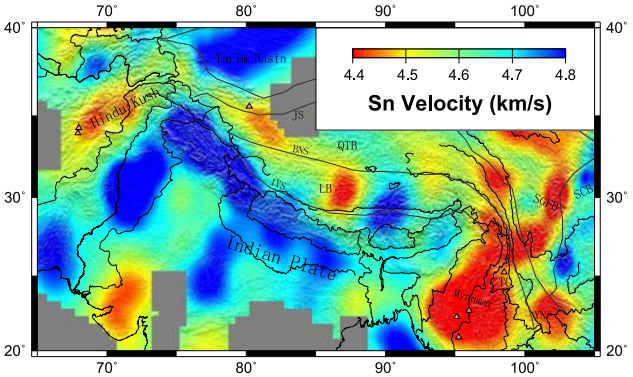

Fig. 7. S_n lateral velocity variations. Red and blue areas correspond to velocities, triangles denote volcanoes, and black lines represent the tectonic line.

such as the Tibetan Plateau and Pamir, the station delays are generally positive. In areas with thinner crusts, such as the Ganges Plain, etc., the station delays are negative. The station and event delays accommodate variations in crustal velocity and thickness and source uncertainties in the inversion.

Figure 7 shows the S_n velocity variations in the study area. The average S_n velocity in the region is about 4.6 km/s. There are obvious variations in different areas: the velocity in the Indian plate, Tarim Basin, and Sichuan Basin can reach 4.8 km/s, and that in the Hindu–Kush, Myanmar, Songpan–Ganzi fold belt (SGFB), and north of the Indus–Yarlung Zangbo suture (IYS), can reach 4.4 km/s.

The inversion result shows significant S_n velocity variations around the Himalayan collision zone, the eastern and western Himalayan syntaxis, and surrounding regions. Low S_n velocities are found in the Myanmar region. Considering the high surface heat flow in this region, we infer that these low-velocity anomalies are associated with the high temperatures or partial melting at the uppermost mantle (Hearn and Ni, 1994; Hu *et al.*, 2001). The hot material backarc upwelling may come from the lithosphere of the Indian plate which subducted into the upper mantle or deeper part. A similar situation is found in the Hindu–Kush region, in which the Indian plate subducts to the mantle of this area from the southeast (Zang *et al.*, 1992). The low S_n velocity in this area provides more evidence of the subduction.

The collision between the Indian and Eurasian plates in the Himalayan region is widely accepted, but there are still many different opinions regarding the mechanism of the collision and the subduction. In the inversion result, the northward high-velocity area of the Indian plate roughly reaches the northern part of the IYS, and there are low-S_n-velocity zones in the Lhasa and Qiangtang blocks. The low-velocity anomaly in the western Qiangtang block was also obtained by previous studies, but the velocity distribution of the Lhasa block is different (Hearn *et al.*, 2004; Pei *et al.*, 2007). The ray coverage of the dataset of the previous study is not good and the resolution is low. Better ray path coverage and spatial resolution suggest that our result is plausible. The INDEPTH-III study proposed that the Indian lithosphere stretches northward, and that the lower lithosphere subducts into the mantle under 32°N by a larger angle (Zhao *et al.*, 2004). The numerical calculation results of the two-dimensional thermal structure of the lithosphere show that the temperature of the Moho in this area is high, and that the lithosphere reaches the temperature of partial melting (Zhou, 2000). The INDEPTH-IV study interpreted either a piece of Lhasa Terrane or remnant oceanic slab underthrust below northern Tibet (Yue *et al.*, 2012). Our inversion results support the idea that the uppermost mantle of the Lhasa and western Qiangtang blocks has high temperatures or partial melting, which causes the low S_n velocity. This phenomenon may be related to the hot material upwelling caused by the subduction of the Indian lithosphere. This result can explain the serious attenuation of the *S* wave in the Qiangtang block (Ni and Barazangi, 1983; Rapine *et al.*, 1997). It is also consistent with L_g attenuation, low *P* wave velocity, low *Q* value, low resistivity, and other geophysical observations in this region (McNamara *et al.*, 1995; Wittlinger *et al.*, 1996; Fan and Lay, 2002; Unsworth *et al.*, 2005). The east–west variability of the S_n velocity beneath southern Tibet indicates that the underthrusted Indian continental lithosphere is not a homogeneous body but rather in a piecewise manner. This conjecture is consistent with those of other researchers (Lü *et al.*, 2011; Liang *et al.*, 2012). A high S_n velocity is found in the Tarim and Sichuan Basins, which have a cold lithosphere and stable tectonics. A significantly low S_n velocity is found at the Songpan-Ganzi orogenic belt. This finding is consistent with the results of *P*-wave inversion in previous studies (Liang and Song, 2006; Liang *et al.*, 2011). At the edge of the present study area, the inversion resolution is limited by sparse ray coverage and the results are not discussed.

A comparison of the S_n velocity distribution with previously-obtained P_n tomography results (Lü *et al.*, 2011) reveals that the high- and low-velocity anomaly areas of the S_n and P_n waves are consistent. Tectonically stable areas such as the Tarim Basin, the Sichuan Basin, and the Indian plate, have high P_n and S_n velocities. The Hindu-Kush and Myanmar regions, as well as the Songpan-Ganzi orogenic belt, have low P_n and S_n velocities. Given that two independent data sets of the inversion of the P_n and S_n travel-time data yield similar results which coincide with each other, the credibility of the inversion results is confirmed. In regions with low P_n velocities, a low S_n velocity is more obvious, showing that the shear wave velocity is more sensitive to the influence of temperature and pressure conditions. The S_n model of the China region obtained by Pei *et al.* (2007) showed low velocity anomalies at Yunnan, SGFB, and the western Qiangtang block, and a high velocity anomaly at Sichuan Basin which are similar to our model. The velocity anomaly at the Lhasa block, and the high velocity of India and low velocity of the Hindu–Kush region of our model, were not obtained by the previous study.

There is only minimal heat flow data observed in the Tibetan Plateau region. In the compilation of heat flow data in the China continental area (Wang and Huang, 1990), the measured value of the terrestrial heat flow within the vicinity of the Tibet 90°E area is larger than the average value in China. However, the S_n velocity of this area is high. We infer that this area can be represented with a tectonic model of a hot crust and a cold mantle. The surface heat flow may not come from the mantle but from the crust. The difference between the thermal tectonics of the crust and upper mantle suggests a potential decoupling between the crust and upper mantle. It also supports the idea that crustal material flow may occur in this region (Bai *et al.*, 2010; Zhang *et al.*, 2010b).

5. Conclusions

We imaged S_n velocity variations beneath the Himalayan collision zone and the surrounding regions using seismic travel-time data. The average S_n velocity in the study area is 4.6 km/s. The maximum velocity perturbation is approximately 0.2 km/s. High-velocity structures are found under the Indian plate, Tarim Basin, and Sichuan Basin, whereas low S_n velocities are found beneath the Myanmar region, the Hindu Kush region, and the Lhasa block and Qiangtang block. A comparison of the S_n velocity distribution

with previously obtained P_n tomography results reveals that the high- and low-velocity anomaly areas of the S_n and P_n waves are consistent. The low S_n velocity anomalies are more obvious than the P_n ones. Our results support the idea that the lithosphere of the Indian plate subducted into the mantle and caused hot material upwelling. The low-velocity anomalies are due to the high temperature or partial melting at the uppermost mantle. The high S_n velocity anomalies of the Indian Plate and the low anomalies in the Tibetan Plateau are discontinuous in the east–west direction, indicating that the Indian plate probably subducts in a piecewise manner. The difference between the thermal tectonics of the crust and upper mantle in southern Tibet supports the idea that crustal material flow may occur in this region. The S_n velocity tomography result provides a seismological basis for the study of plate tectonics and geodynamic processes in this region.

Acknowledgments. We thank Professor Thomas Hearn for providing the original tomographic codes. We appreciate the insightful suggestions by two reviewers and the associate editor. All figures were prepared using the Generic Mapping Tolls (Wessel and Smith, 1998). This study was supported by the China Postdoctoral Science Foundation 2012M510043 and 2013T60166, the National Nature Science Foundation of China (Grant Nos. 41074031, 40940021, 41174036), the China Earthquake Program 200808078 and the CAS/SAFEA International Partnership Program for Creative Research Teams (Grant No. KZZD-EW-TZ-05).

References

Bai, D., M. Unsworth, M. Meju, X. Ma, J. Teng *et al*., Crustal deformation of the eastern Tibetan plateau revealed by magnetotelluric imaging, *Nat. Geosci*., **3**, 358–362, doi:10.1038/ngeo830, 2010.

Ding, L., P. Kapp, D. Zhong, and W. Deng, Cenozoic volcanism in Tibet: Evidence for a transition from oceanic to continental subduction, *J. Petrol*., **44**(10), 1833–1865, doi:10.1093/petrology/egg061, 2003.

Fan, G. and T. Lay, Characteristics of Lg attenuation in the Tibetan Plateau, *J. Geophys. Res*., **107**(B10), 2256, doi:10.1029/2001JB000804, 2002.

Goes, S., R. Govers, and P. Vacher, Shallow mantle temperatures under Europe from P and S wave tomography, *J. Geophys. Res*., **105**(B5), 11153–11169, 2000.

Hearn, T., Anisotropic Pn tomography in the western United States, *J. Geophys. Res*., **101**, 8403–8414, 1996.

Hearn, T. and J. Ni, Pn velocities beneath continental collision zones, the Turkish-Iranian plateau, *Geophys. J. Int*., **117**, 273–283, 1994.

Hearn, T., S. Wang, J. Ni, Z. Xu, Y. Yu, and X. Zhang, Uppermost mantle velocities beneath China and surrounding regions, *J. Geophys. Res*., **109**, B11301, doi:10.1029/2003JB002874, 2004.

Hu, S., L. He, and J. Wang, Compilation of heat flow data in the China continental area (3rd edition), *Chinese J. Geophys*., **44**(5), 611–626, 2001.

Huang, J. and D. Zhao, High-resolution mantle tomography of China and surrounding regions, *J. Geophys. Res*., **111**, B09305, doi:10.1029/2005JB004066, 2006.

Kind, R., X. Yuan, J. Saul, D. Nelson, S. V. Sobolev, J. Mechie, W. Zhao, G. Kosarev, J. Ni, U. Achauer, and M. Jiang, Seismic images of crust and upper mantle beneath Tibet: Evidence for Eurasian plate subduction, *Science*, **298**, 1219–1221, 2002.

Liang, C. and X. Song, A low velocity belt beneath northern and eastern Tibetan Plateau from Pn tomography, *Geophys. Res. Lett*., **33**, L22306, doi:10.1029/2006GL027926, 2006.

Liang, C., X. Song, and J. Huang, Tomographic inversion of Pn travel times in China, *J. Geophys. Res*., **109**, B11304, doi:10.1029/2003JB002789, 2004.

Liang, X., Y. Shen, Y. Chen, and Y. Ren, Crustal and mantle velocity models of southern Tibet from finite frequency tomography, *J. Geophys. Res*., **116**, B02408, doi:10.1029/2009JB007159, 2011.

Liang, X., E. Sandvol, Y. Chen, T. Hearn, J. Ni, S. Klemperer, Y. Shen, and F. Tilmann, A complex Tibetan upper mantle: A fragmented Indian slab and no south-verging subduction, *Earth Planet. Sci. Lett*., **333–334**, 101–111, 2012.

Lü, Y., S. Ni, B. Liu, and Y. Sun, Pn tomographic velocity and anisotropy beneath the Tibetan Plateau and the adjacent regions, *Earth Planets Space*, **63**(11), 1169–1173, doi:10.5047/eps.2011.07.013, 2011.

Lü, Y., B. Liu, S. Pei, Y. Sun, M. Toksöz, and X. Zeng, Pn tomographic velocity and anisotropy beneath the Iran region, *Bull. Seismol. Soc. Am*., **102**(1), 426–435, doi:10.1785/0120100141, 2012.

McNamara, D., T. Owens, and W. Walter, Observations of regional phase propagation across the Tibetan plateau, *J. Geophys. Res*., **100**, 22215–22229, 1995.

Molnar, P. and P. Tapponnier, Cenozoic tectonics of Asia: Effects of a continental collision, *Science*, **189**, 419–426, 1975.

Ni, J. and M. Barazangi, High-frequency seismic wave propagation beneath the Indian Shield, Himalayan Arc, Tibetan Plateau and surrounding regions: High uppermost mantle velocity and efficient Sn propagation beneath Tibet, *Geophys. J. R. Astron. Soc*., **72**, 665–689, 1983.

Nolet, G. and A. Ziehuis, Low S velocities under the Tomquist Teisseyre zone: Evidence for water injection into the transition zone by subduction, *J. Geophys. Res*., **99**, 15813–15820, 1994.

Paige, C. and M. Saunders, LSQR, An algorithm for sparse linear equations and sparse linear system, *ACM Trans. Math. Software*, **8**, 43–71, 1982.

Pei, S. and Y. Chen, Link between seismic velocity structure and the 2010 Ms 7.1 Yushu earthquake, Qinghai, China: Evidence from aftershock tomography, *Bull. Seismol. Soc. Am*., **102**, 445–450, 2012.

Pei, S., J. Zhao, Y. Sun, Z. Xu, S. Wang, H. Liu, C. Rowe, M. Toksöz, and X. Gao, Upper mantle seismic velocities and anisotropy in China determined through Pn and Sn tomography, *J. Geophys. Res*., **112**, B05312, doi:10.1029/2006JB004409, 2007.

Pei, S., Y. Sun, M. Toksöz, Y. Chen, X. Gao, Z. Wang, J. Zhao, and H. Liu, Imaging poisson's ratio of the uppermost mantle beneath China, *Bull. Seismol. Soc. Am*., **101**, 1452–1461, 2011a.

Pei, S., Y. Sun, and M. Toksöz, Tomographic Pn and Sn Velocity beneath Continental Collision Zone from Alps to Himalaya, *J. Geophys. Res*., **116**, B10311, doi:10.1029/2010JB007845, 2011b.

Phillips, W., M. Begnaud, C. Rowe, L. Steck, S. Myers, M. Pasyanos, and S. Ballard, Accounting for lateral variations of the upper mantle gradient in Pn tomography studies, *Geophys. Res. Lett*., **34**, L14312, doi:10.1029/2007GL029338, 2007.

Rapine, R., J. Ni, and T. Hearn, Regional wave propagation in China and its surrounding regions, *Bull. Seismol. Soc. Am*., **87**, 1622–1636, 1997.

Ren, Y. and Y. Shen, Finite frequency tomography in southern Tibet: Evidence for the causal relationship between mantle lithosphere delamination and the north-south trending rifts, *J. Geophys. Res*., **113**, B10316, doi:10.1029/2008JB005615, 2008.

Sun, Y., M. Toksöz, S. Pei, D. Zhao, F. Morgan, and A. Rosca, S-wave tomography of the crust and uppermost mantle in China, *J. Geophys. Res*., **113**, B11307, doi:10.1029/2008JB005836, 2008.

Teng, J., Z. Yin, H. Liu, Z. Zhang, J. Hu, K. Sun, and J. Wei, The 2D and 3D lithosphere structure and continental dynamics of Qinghai-Xizang Plateau, *Chinese J. Geophys*., **A02**, 117–130, 1994.

Teng, J., Z. Zhang, G. Wang, H. Liu, J. Hu *et al*., The deep internal dynamical processes and new model of continental-continental collision in Himalayan collision orogenic zone, *Chinese J. Geophys*., **42**(4), 481–494, 1999.

Unsworth, M., A. Jones, W. Wei, G. Marquis, S. Gokarn, and J. Spratt, Crustal rheology of the Himalaya and southern Tibet inferred from magnetotelluric data, *Nature*, **438**, 78–81, doi:10.1038/nature04154, 2005.

Wang, J. and S. Huang, Compilation of heat flow data in the China continental area (2nd edition), *Seismol. Geol*., **12**(4), 351–366, 1990.

Wang, Q., P. Zhang, J. Freymueller, R. Bilham, K. Larson *et al*., Present-day crustal deformation in China constrained by global positioning system measurements, *Science*, **294**, 574–577, 2001.

Wessel, P. and W. Smith, New, improved version of Generic Mapping Tools released, *Eos Trans. AGU*, **79**(47), 579, 1998.

Wittlinger, G., F. Masson, G. Poupinet, P. Tapponnier, J. Mei *et al*., Seismic tomography of northern Tibet and Kunlun: Evidence for crustal blocks and mantle velocity contrasts, *Earth Planet. Sci. Lett*., **139**, 263–279, 1996.

Xu, G., H. Yao, L. Zhu, and Y. Shen, Shear wave velocity structure of the crust and upper mantle in western China and its adjacent area, *Chinese J. Geophys*., **50**(1), 193–208, 2007.

Yao, Z., R. Roberts, and A. Tryggvason, Calculating resolution and covariance matrices for seismic tomography with the LSQR method, *Geophys. J. Int*., **138**, 886–894, 1999.

Yue, H., Y. Chen, E. Sandvol, J. Ni, T. Hearn *et al*., Lithospheric and upper

mantle structure of the northeastern Tibetan Plateau, *J. Geophys. Res.*, **117**, B05307, doi:10.1029/2011JB008545, 2012.

Zang, S., Z. Wu, and J. Ning, The interaction of plates around China and its effect on the stress field in China, part II: The influence of Indian Plate, *Chinese J. Geophys.*, **35**(4), 428–440, 1992.

Zeng, R., Z. Ding, Q. Wu, and J. Wu, Seismological evidences for the multiple incomplete crustal subductions in Himalaya and southern Tibet, *Chinese J. Geophys.*, **43**(6), 780–797, 2000.

Zhang, Z. and S. Klemperer, Crustal structure of the Tethyan Himalaya, southern Tibet: New constraints from old wide-angle seismic data, *Geophys. J. Int.*, **181**, 1247–1260, doi:10.1111/j.1365-246X.2010.04578.x, 2010.

Zhang, Z., Y. Deng, J. Teng, C. Wang, R. Gao, Y. Chen, and W. Fan, An overview of the crustal structure of the Tibetan plateau after 35 years of deep seismic soundings, *J. Asian Earth Sci.*, **40**, 977–989, doi:10.1016/j.jseaes.2010.03.010, 2010a.

Zhang, Z., X. Yuan, Y. Chen, X. Tian, R. Kind, X. Li, and J. Teng, Seismic signature of the collision between the east Tibetan escape flow and the Sichuan Basin, *Earth Planet. Sci. Lett.*, **292**, 254–264, doi:10.1016/j.epsl.2010.01.046, 2010b.

Zhang, Z., S. Klemperer, Z. Bai, Y. Chen, and J. Teng, Crustal structure of the Paleozoic Kunlun orogeny from an active-source seismic profile between Moba and Guide in East Tibet, China, *Gondwana Res.*, **19**(4), 994–1007, 2011.

Zhao, D., Global tomographic images of mantle plumes and subducting slabs: Insight into deep Earth dynamics, *Phys. Earth Planet. Inter.*, **146**, 3–34, 2004.

Zhao, W., G. Xue, Z. Wu, X. Zhao, K. Liu *et al.*, Fine velocity structure of the upper mantle beneath the Xizang Plateau from tomography and its geological interpretations, *Chinese J. Geophys.*, **47**(3), 449–458, 2004.

Zheng, H., T. Li, R. Gao, D. Zhao, and R. He, Teleseismic P-wave tomography evidence for the Indian lithospheric mantle subducting northward beneath the Qiangtang terrane, *Chinese J. Geophys.*, **50**(5), 1418–1426, 2007.

Zhou, H., Progress on studies of rheological dynamics of continental lithosphere, *Earth Sci. Frontiers*, **7**, 121–127, 2000.

Y. Lü (e-mail: lvyan@mail.iggcas.ac.cn), B. Liu, S. Ni, and S. Pei